

The Effect of Ferro-Alloy Additions and Depth on the Quality of Underwater Wet Welds

In an effort to improve weld properties, 60 different coating formulations were developed and welds were made at various depths to 300 ft

BY M. D. ROWE, S. LIU, AND T. J. REYNOLDS

ABSTRACT. Underwater wet welding offers significant cost savings over other repair techniques for submerged structures, but the weld metal mechanical properties are not equal to those of surface welds. The problems of porosity and oxidation of the weld pool as underwater depths increased were addressed by additions of manganese, titanium, boron, and rare earth metals (REM) to the coating of a rutile-based SMAW electrode. A test matrix of 60 coating formulations was prepared and test welds were made at four depths: 70, 140, 200, and 300 ft (21, 43, 61, 91 m).

With the addition of titanium, a strong deoxidant, it was possible to control weld metal chemical composition. Low porosity was associated with electrodes that deposited a slag with a basicity index approaching neutral (1.0). Slag basicity may influence transfer of hydrogen to the weld pool and, thus, influence porosity. Addition of titanium and boron produced a microstructure of 60 to 90 vol-% acicular ferrite. Tensile strength increased with the combined addition of manganese, titanium, and boron. The results of this investigation demonstrated some of the adverse effects of increasing underwater depth on weld metal quality can be mitigated by modifications to the electrode coatings.

Introduction

Underwater wet welding with coated electrodes has proven to be a valuable repair process on offshore platforms, piers, ships, and in nuclear power plants. Wet welding is selected over other repair op-

tions because it can be quickly implemented with relatively simple equipment, thereby dramatically reducing repair cost and downtime. Wet welding is being used increasingly as an underwater repair technique due to research and development in recent years leading to improved weld quality.

Although the quality of wet welds has improved, the mechanical properties are still not equal to those exhibited by dry welds. Mechanical properties of underwater wet welds are a strong function of depth, due to increasing oxidation and porosity. The total pressure increases underwater at a rate of one atmosphere for every 33 ft (10 m) of depth. For a given composition of gas over the weld pool, the partial pressures and, therefore, the chemical activities of oxygen and hydrogen increase in direct proportion to the total pressure. Oxidation of the weld pool causes alloying elements with an affinity for oxygen to be increasingly transferred from the weld metal to the slag in the form of oxides. The resulting decrease in manganese content reduces hardenability of the weld metal and promotes a microstructure of coarse-grained primary ferrite with lower strength and toughness than a fine-grained microstructure.

Pores are present to some extent in almost all wet welds, and porosity is one of the key factors that determine the me-

chanical properties of the weld metal. Porosity of underwater wet welds increases dramatically with depth. In an investigation conducted by Suga and Hasui, porosity began to appear in wet welds at depths greater than 15 ft (4.6 m) and exceeded 5% at 150 ft (46 m) (Ref. 1). The maximum porosity allowed for an AWS D3.6 Class B weld, as measured on a metallographic cross section, is 5%. Class B welds are used for less-critical applications where lower ductility and larger discontinuities can be tolerated (Ref. 2). It becomes increasingly challenging to meet the Class B requirements at depths of 200 to 300 ft (61 to 91 m).

The composition of gas contained within the pores of wet welds has been analyzed and reported in the literature. Suga and Hasui found a gas composition of 96% hydrogen with a small amount of carbon monoxide (Ref. 1). Ando and Asahina performed a similar analysis and found the pores contained in excess of 99% hydrogen (Ref. 3). The works of Suga and Hasui, and of Ando and Asahina, suggest porosity in underwater wet welds is caused mainly by hydrogen.

The formation of pores in underwater wet welds by concentration of hydrogen ahead of the solidification front was modeled by Suga (Ref. 4). Suga predicted the critical radius for pore formation would decrease with increasing pressure. The critical radius is the minimum size at which a pore is stable; thus, a smaller critical radius means pores can nucleate more easily. The model developed by Suga is consistent with the observed increase in porosity with depth.

Assuming porosity is caused by hydrogen, techniques to reduce the hydrogen content of wet welds should also be effective in reducing porosity. Sanchez-Osio *et al.*, decreased porosity in wet welds from 2.2 to 1.0% at a depth of 30 ft (9 m) by increasing calcium carbonate in the coating from 9 to 12.5% (Ref. 5). Carbonates decompose to form carbon diox-

KEY WORDS

Coated Electrodes
Ferro Alloy
Hydrogen
Oxygen
Porosity
Underwater
Wet Welding

M. D. ROWE is with Haynes International, Inc., Kokomo, Ind. S. LIU is with the Center for Welding, Joining, and Coatings Research, Colorado School of Mines, Golden, Colo. T. J. REYNOLDS is with Global Divers and Contractors LLC, Division of Global Industries LTD., New Iberia, La.

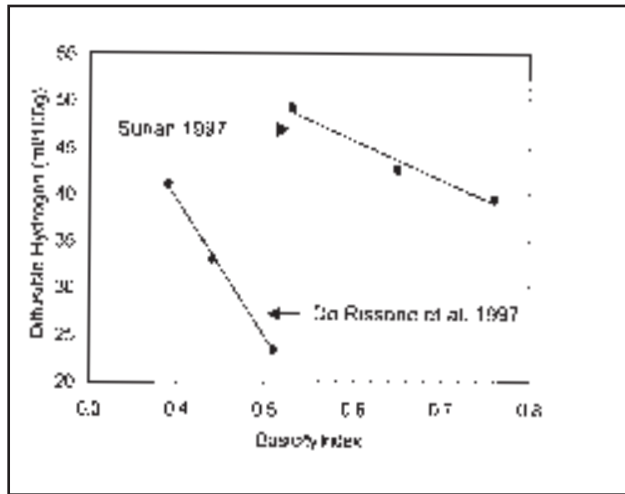


Fig. 1 — Diffusible hydrogen as a function of slag basicity for a rutile-based electrode deposited in air (Refs. 9, 10).

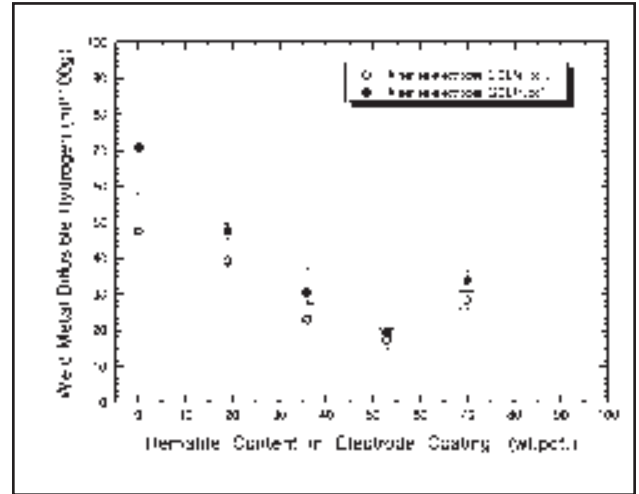
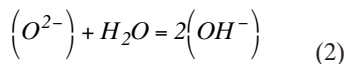
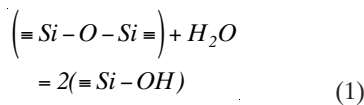


Fig. 2 — Diffusible hydrogen as a function of increasing hematite addition to an acid-type electrode coating (increasing slag basicity) for underwater wet welds (Ref. 6).

ide and carbon monoxide in the arc, reducing the partial pressure of hydrogen, thus reducing the equilibrium concentration of hydrogen in the weld pool.

In addition to carbonate content, it has been shown slag basicity can influence the hydrogen content of weld metal. Medeiros and Liu demonstrated the weld metal hydrogen pickup in underwater wet welding was strongly dependent on water vapor solubility in slags (Ref. 6). In many slag systems, there is a minimum in water vapor solubility near neutral basicity. Water vapor dissolves in slags according to Equation 1 in acid melts and Equation 2 in basic melts (Ref. 7).



Equation 1 represents the breakdown of silicate networks by hydroxyl ions in an acid slag. Equation 2 represents the reaction of water vapor with free oxygen ions in a basic slag. In a slag of neutral basicity, neither of the above mechanisms is favored and the solubility of water vapor in the slag is minimized. The basicity index proposed by Tuliani *et al.*, Equation 3, gives a ratio of network modifiers to network formers, thus giving an approximate numerical value to the degree of polymerization in a complex oxide melt (Ref. 8).

$$BI = \frac{\text{CaO} + \text{CaF}_2 + \text{MgO} + \text{K}_2\text{O} + \text{Na}_2\text{O} + \text{Li}_2\text{O} + \frac{1}{2}(\text{MnO} + \text{FeO})}{\text{SiO}_2 + \frac{1}{2}(\text{Al}_2\text{O}_3 + \text{TiO}_2 + \text{ZrO}_2)} \quad (3)$$

The concept of slag basicity was originally used to predict the partitioning of sulfur between metal and slag in iron and steel making. As an indicator of the structure of the slag, it can be expected various types of slag/metal reactions can be correlated to the basicity index. In welding literature, the slag basicity has been shown to correlate weld metal chemical composition, specifically oxygen and sulfur, to the chemical composition of the slag.

Surian (Ref. 9) and De Rissone *et al.* (Ref. 10), have shown that increasing the slag basicity of rutile-based coated electrodes toward a more neutral value results in lower diffusible hydrogen for similar moisture contents, as seen in Fig. 1. Medeiros and Liu have shown the diffusible hydrogen content of underwater wet welds goes through a minimum with increasing additions of hematite to an acid electrode coating, as seen in Fig. 2. A similar trend was noted for total (diffusible plus residual) hydrogen (Ref. 6). Hematite decomposes to form FeO in the slag, thus increasing slag basicity. Assuming the porosity of wet welds is caused by hydrogen and weld metal hydrogen is influenced by slag basicity, it can be expected slag basicity will influence the porosity of underwater wet welds.

Other mechanisms for pore formation have been proposed. Liu *et al.* proposed

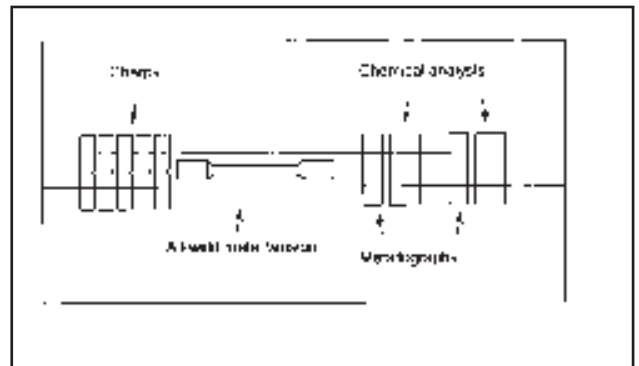


Fig. 3 — Orientation of test specimens removed from the V-groove welds.

that oxidation of carbon and hydrogen in the weld pool can cause porosity by formation of carbon monoxide and water vapor (Ref. 11). The authors went on to suggest steam in the pores can react with the surrounding iron to form iron oxide and hydrogen, thus explaining the presence of hydrogen, not water vapor, in the pores. It was concluded if the weld pool were sufficiently deoxidized, porosity due to both carbon monoxide and steam could be prevented (Ref. 11). Research into means of controlling the transfer of oxygen and hydrogen to the weld pool is critical to further improve the mechanical properties of underwater wet welds.

Experimental Procedures

The objective of the present investigation was to improve the quality of wet welds by optimization of the ferro-alloy additions to the electrode coating for given depths. The addition of certain al-

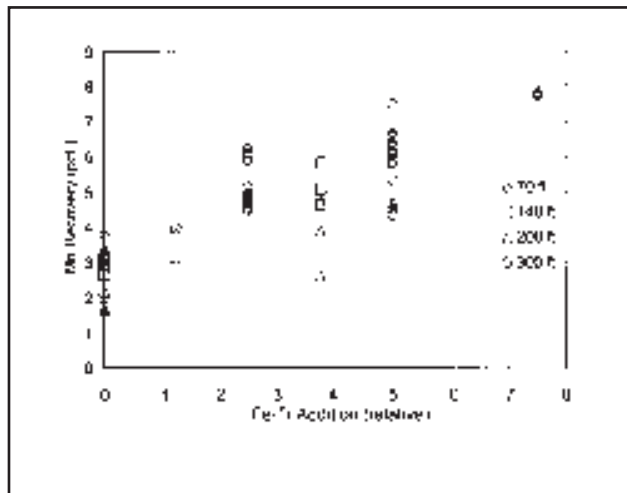


Fig. 4 — Percent recovery of manganese from the coating to the steel weld metal as a function of ferro-titanium addition to a rutile-based electrode coating.

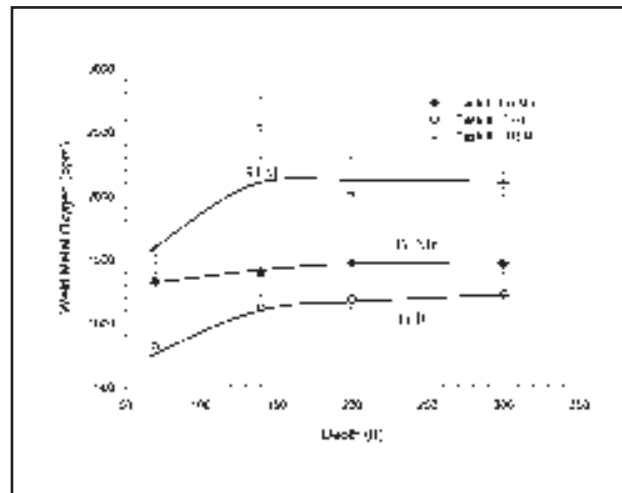


Fig. 5 — Effect of ferro-alloy additions to a rutile-based coating on the weld metal oxygen content of the V-groove welds.

Table 1 — Chemical Composition of Steel Base Plates and Core Wire

	C wt-%	Mn wt-%	Si wt-%	Ti (ppm)	B (ppm)
Test welds	0.14–0.22	0.6–0.8	0.21	<100	<5
V-groove	0.05	1.51	0.4	<100	5
Core wire	0.01	0.15	0.02	<100	<5

Table 2 — Welding Parameters for Test Welds and V-Groove Welds

	Test Welds	V-Groove Welds
Position	1G	3G ^(a)
Polarity	DCEP	DCEP
Current (A)	165–190	160–180
Voltage (V)	24–32	22–34
Travel, in./min (mm/s)	14–19 (5.9–8.0)	8–18 (3.4–7.6)
Heat input, kJ/in. (kJ/mm)	14–26 (0.6–1.0)	14–30 (0.6–1.2)

(a) Downhill progression.

loying elements was expected to counter the oxidizing effects of water, allowing better control over the oxygen content, chemical composition, and microstructure of the weld metal. By adding deoxidants of increasing strength to the weld pool, it was expected any porosity caused by oxidation of carbon or hydrogen would be eliminated. The present investigation was organized into three tasks to address the problems associated with increasing underwater depth.

Task 1 involved increasing additions of ferro-manganese, Task 2 involved addi-

tion of ferro-titanium and ferro-boron, and Task 3 involved addition of ferro-silicon-rare-earth-metal (REM) alloy to the electrode coating. In Task 1, the coating ferro-manganese content was increased to compensate for the reduced recovery of manganese with depth due to oxidation. In Task 2, titanium and boron were added to promote a microstructure of fine acicular ferrite in the weld metal. Titanium and the rare earth metals, cerium and lanthanum, are strong deoxidants and were expected to reduce the weld metal oxygen content, eliminate any porosity caused by oxidation reactions, and improve the recovery of alloying elements. Microstructural refinement through increased manganese content and titanium-boron additions was expected to improve toughness and increase strength.

A rutile-based electrode coating was used as the baseline formulation. The excellent arc stability and slag characteristics of rutile-based electrodes make them the most popular choice for underwater wet welding. The exact coating formulation is proprietary to the project sponsors and cannot be provided. The mineral ingredients of the coating were reduced proportionally to accommodate the increased ferro-alloy additions.

The coatings were extruded onto a 1/8-in.-diameter (3.2-mm) steel core wire with a coating diameter of 1/2 in. (5.6 mm) by a commercial manufacturer of welding electrodes. The composition of the core wire is given in Table 1. The finished electrodes were shipped to an offshore contractor where a waterproof coating was applied and the experimental welds were produced.

Test welds were produced at depths of

70, 140, 200, and 300 ft (21, 43, 61, 91 m). The test welds consisted of a three-layer, bead-on-plate deposit with a total of nine passes. After analysis of the test welds, one composition from each of the three tasks was selected for each depth and V-groove welds were prepared. The weld preparation was a 3/8-in.-deep (16-mm) V-groove with a 60-deg included angle milled into a 1-in.-thick plate. The compositions of the base metals are provided in Table 1. Approximately 24 to 31 passes were required to complete the V-grooves. Welding was conducted in a hyperbaric chamber pressurized to simulate the appropriate underwater depth. Welding parameters are given in Table 2. Manual welding was performed by qualified professional diver/welders.

V-groove welds were radiographed by an independent laboratory and film was interpreted according to the AWS D3.6 specification (Ref. 2) by an ASNT Level II radiographic inspector.

Porosity and top-bead microstructure were quantified using standard metallographic techniques. Two cross sections from each weld were examined. Area percent porosity was measured at 10X magnification with an overlaid grid. The average and 90% confidence interval of four areas were reported. Quantitative metallography was performed on the top bead microstructure etched with 2% nital. A total of six to ten photomicrographs were examined from each weld taken from two cross sections. The microstructures were classified according to the IIW classification scheme for steel weld metal as PF (primary ferrite), FS (ferrite with second phase aligned or non-aligned), and AF (acicular ferrite) (Ref. 12). A 1000-point count on each weld was

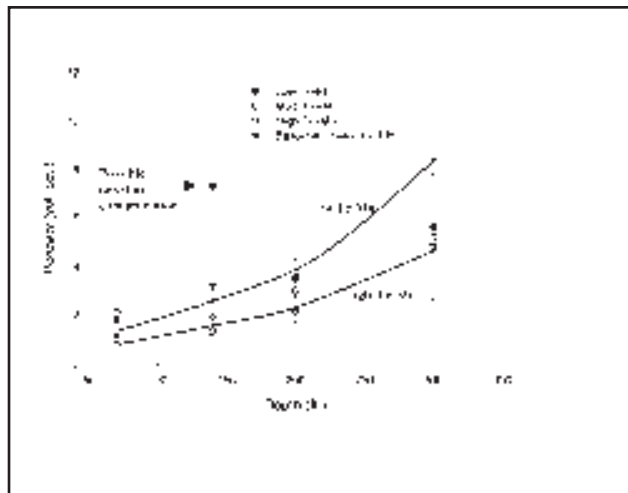


Fig. 6 — Porosity as a function of depth and ferro-manganese addition for Task 1 test welds.

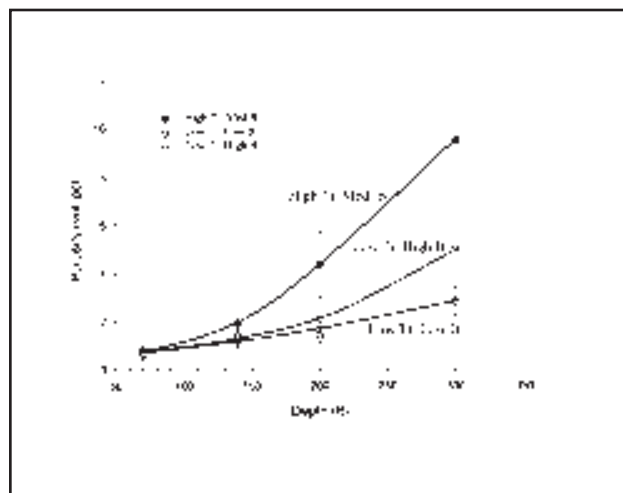


Fig. 7 — Weld metal porosity as a function of depth and addition of titanium and boron to the coating for selected Task 2 test welds.

performed to quantify the proportions of the microstructural constituents.

To quantify the effect of ferro-alloy additions on the reheated microstructure, the average ferrite grain size of the reheated weld metal was measured with an image analyzer. The average linear-intercept grain size was measured on at least 15 fields from each weld at a magnification of 500X. The grain size varied significantly from the coarse-grained reheated zone (CGRHZ) to the fine-grained reheated zone (FGRHZ) within a given weld. The average grain size was measured by making a traverse of 5 fields from the CGRHZ to the FGRHZ of the top bead. Three such traverses were made for a total of 15 fields and the average and 90% confidence interval of the 15 measurements were reported.

Weld metal chemical compositions were measured by optical-emission spectroscopy at two locations from each weld and the average was reported. A procedure was developed to produce a flat, pore-free surface on the top bead by peening with a ball-peen hammer, then grinding lightly to clean up the surface. Peening closed surface porosity and improved the accuracy of the analysis. Oxygen and nitrogen were measured by combustion analysis. Five samples from each weld were tested to give a reasonable level of confidence. The average and 90% confidence interval were reported.

Chemical analysis of slags was performed by an independent commercial lab using photo-optical-emission spectroscopy. Slag samples were crushed on a steel plate and metallic particles were removed magnetically prior to analysis.

Mechanical properties were measured using tensile and Charpy V-notch

impact toughness testing. An all-weld-metal tensile bar with a 1/4-in.-round (6.4-mm) reduced section was removed from each V-groove weld. Five full-size Charpy impact test bars were broken at 28°F (-2°C) in accordance with the AWS D3.6 specification (Ref. 2). Percent shear fracture was measured in a scanning electron microscope, neglecting the area occupied by porosity. Orientation of test specimens removed from the V-groove welds is shown in Fig. 3.

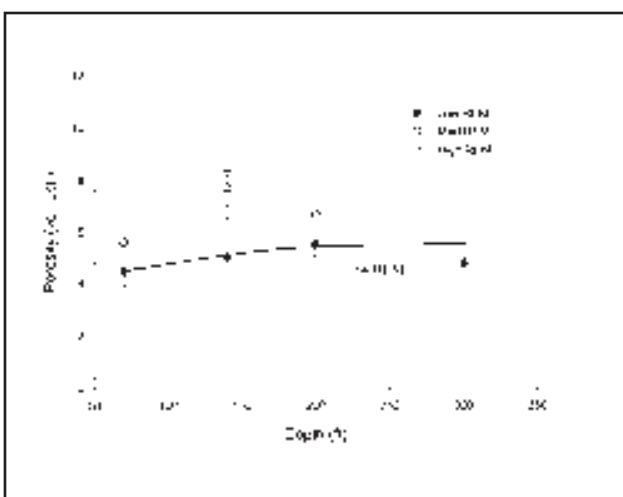


Fig. 8 — Weld metal porosity as a function of depth and REM addition to a rutile-based coating.

Results and Discussion

Chemical Composition of Welds

Results of weld metal chemical analyses are given in Tables 3 through 8. The first number of the formulation IDs given in the tables indicates the test depth, the letters F, T, B, and R indicate the type of ferro-alloy addition, Fe-Mn, Fe-Ti, Fe-B, and Fe-Si-REM, respectively, and the number following the letter indicates increasing levels of addition from 1 to 3. The weld metal manganese content remained approximately constant over the range of ferro-manganese addition tested. A 16% increase in ferro-manganese addition to the coating over the baseline addition produced

a 0.3 wt-% increase in manganese content for welds made in air. A 28% increase in ferro-manganese addition failed to produce any increase in weld metal manganese content of the underwater wet welds. The failure of ferro-manganese additions to increase the weld metal manganese content was due to the strongly oxidizing underwater environment.

Titanium has a stronger affinity for oxygen than iron, manganese, or boron. As a result, titanium was expected to increase the recoveries of the weaker oxide formers by combining preferentially with oxygen. The addition of titanium had a strong effect on the recovery of both manganese and boron. The effect of titanium addition on manganese recovery can be seen in Fig. 4 and a similar trend was ob-

Table 3 — Analysis of Steel Test Welds with Increasing Fe-Mn Additions

ID	Depth (ft)	C (wt-%)	Mn (wt-%)	Si (wt-%)	O (ppm)	Porosity		Microstructure			
						+/-	(%)	PF (%)	FS (%)	AF (%)	
1F1	70	0.05	0.47	0.24	1174	69	1.8	0.7	31	58	11
1F2	70	0.04	0.45	0.24	1160	66	2.1	0.2	33	52	15
1F3	70	0.06	0.42	0.19	1125	60	0.8	0.3	24	53	21
2F1	140	0.04	0.40	0.32	1433	93	7.3	3.1	22	63	15
2F2	140	0.04	0.42	0.16	1264	44	1.3	0.3	27	55	17
2F3	140	0.04	0.42	0.22	976	123	1.9	0.9	34	51	15
3F1	200	0.05	0.46	0.24	1476	112	3.5	0.4	30	51	19
3F2	200	0.04	0.25	0.12	1650	142	3.0	1.3	42	44	14
3F3	200	0.04	0.26	0.13	1215	53	2.1	0.6	36	40	20
4F1	300	0.06	0.43	0.28	1397	266	5.6	2.3	30	57	12
4F2	300	0.06	0.26	0.13	1137	39	5.2	2.6	30	53	17
4F3	300	0.05	0.33	0.14	1290	131	4.8	1.8	34	46	21

Table 4 — Analysis of Steel V-Groove Welds with Increasing Fe-Mn Additions

ID	Depth (ft (m))	C (wt-%)	Mn (wt-%)	Si (wt-%)	O (ppm)	Porosity		Microstructure		
						+/-	(%)	PF (%)	FS (%)	AF (%)
1F3	70 (21)	0.04	0.69	0.30	1328	145	2.5	27	58	15
2F3	140 (43)	0.05	0.49	0.21	1390	176	1.9	45	48	7
3F3	200 (61)	0.05	0.47	0.26	1470	76	1.5	33	61	5
4F2	300 (91)	0.05	0.50	0.24	1462	76	2.3	53	42	5

served for boron recovery. In the present discussion, the recovery of an alloying element is defined as the wt-% of the alloying element in the weld deposit divided by the wt-% of the ferro-alloy addition to the coating multiplied by 100%. At 70 ft (21 m), manganese recovery increased from approximately 3.5% to nearly 8% over the range of ferro-titanium addition tested. At greater depths, manganese recovery also increased with ferro-titanium addition, but to a lesser extent than at 70 ft. Boron recovery doubled over the range of ferro-titanium addition tested.

Because rare earth metals (REM) have a much higher affinity for oxygen than manganese, boron, or titanium, the recoveries of other alloying elements were expected to increase with addition of REM-ferro-silicon. Preliminary test welds produced at a depth of 1.5 ft (0.5 m) produced a significant increase in the recoveries of manganese and boron with the rare earth metal addition, but subsequent trials at greater depths failed to reproduce the effect. The increasingly oxidizing nature of the environment at greater depths may have exceeded the ability of the added REM to protect the other alloying elements from oxidation.

Oxygen

The effectiveness of ferro-alloy additions at reducing weld metal oxygen con-

tent was anticipated to correspond to the relative thermodynamic stability of the oxides. Strong deoxidants form oxides in the weld pool, which may float out into the slag, thereby removing oxygen from the weld pool. However, the oxides may become trapped during solidification in the form of oxide inclusions, resulting in a high weld metal oxygen content. Thus, the use of deoxidants to reduce the weld metal oxygen content can be complex.

Manganese has a higher affinity for oxygen than iron. In general, the highest ferro-manganese additions produced slightly lower oxygen levels than the lowest ferro-manganese additions, although the trend was not strong. With addition of titanium, control of the oxygen content should be determined by titanium oxidation rather than oxidation of manganese. For the V-groove welds, titanium-boron additions produced weld metal with significantly lower oxygen content at all depths than with addition of only ferro-manganese, as seen in Fig. 5. A 40% reduction in weld metal oxygen content was achieved at 70 ft (21 m) water depth.

REM additions were expected to reduce weld metal oxygen content due to the high affinity of REM for oxygen. In preliminary test welds at a depth of 1.5 ft (0.5 m), weld metal oxygen was reduced by 25% over the range of REM additions tested, but a similar reduction in oxygen content was not observed in test welds produced at greater depths. In fact, the

opposite trend occurred; weld metal oxygen content increased with increasing levels of REM addition. Weld metal oxygen contents were significantly higher with REM additions than with titanium-boron or manganese additions, as seen in Fig. 5. Contrary to expectations based on the thermodynamic stability of REM oxides and preliminary testing at a shallow depth, addition of REM was not effective as a deoxidant.

Weld Metal Nitrogen Content

Weld metal nitrogen content was measured to ensure the ferro-alloys had not picked up excessive quantities of nitrogen in storage. Nitrogen contents were in the range of 50 to 70 ppm for welds with manganese and REM additions, and 60 to 110 ppm for welds with titanium-boron additions. The weld metal nitrogen contents were at a low enough level that the observed porosity was not likely to have been caused by nitrogen contamination.

Porosity

Results of metallographic porosity measurements are given in Tables 3 through 8. Higher levels of ferro-manganese addition produced less porous welds in most cases, as seen in Fig. 6. The reduction in porosity is not greater than the 90% confidence interval on the four areas measured, indicating there is variation in the amount of porosity from one location in the weld to another. Despite the scatter in the individual measurements at the 300 ft (91 m) water depth, the higher levels of ferro-manganese addition reduced porosity to less than 5% on a macro cross section, which is a requirement for an AWS D3.6 Class B weld. One of the long-term goals of the underwater wet welding community has been to consistently produce Class B welds at water depths of 200 to 300 ft (61 to 91 m).

Weld metal porosity increased as a function of increasing titanium and boron additions, as seen in Fig. 7. Smaller error bars than in Fig. 6 indicate the pores are smaller and more uniformly distributed throughout the weld. For a given volume fraction porosity, a uniform distribution of small pores is more desirable than a few large pores that occur in groups. Controlled additions of titanium and boron assist in meeting quality requirements by reducing pore size, but excessive additions increase volume-percent porosity.

There was a trend of increasing porosity with greater additions of REM, as shown in Fig. 8. Addition of REM to the coating increased both porosity and oxidation of the weld metal, suggesting exposure of the weld pool to water was in-

Table 5 — Analysis of Steel Test Welds with Ti-B Additions

ID	Depth ft (m)	C wt-%	Mn wt-%	Ti ppm	B ppm	O ppm	+/-	Hardness			Porosity		Microstructure		
								Avg (HV)	+/-	Max.	Avg (%)	+/-	PF (%)	FS (%)	AF (%)
1T1B1	70 (21)	0.06	0.86	125	18	875	7	304	5	322	0.6	0.5	20	3	77
1T1B2	70 (21)	0.06	0.72	310	18	912	124	301	12	340	1.1	0.5	10	1	90
1T1B3	70 (21)	0.06	0.91	150	48	887	29	321	7	340	0.8	0.2	5	40	55
1T2B1	70 (21)	0.05	0.61	165	8	966	76	283	6	302	1.9	0.9	30	10	60
1T2B2	70 (21)	0.06	0.83	280	20	797	25	305	4	316	0.7	0.2	15	4	81
1T2B3	70 (21)	0.05	0.67	175	25	1005	46	277	6	297	2.2	0.4	18	2	82
1T3B1	70 (21)	0.06	0.66	305	11	929	29	296	7	317	3.7	0.8	11	3	86
1T3B2	70 (21)	0.06	0.66	400	22	911	48	292	7	311	4.7	1.7	10	2	89
1T3B3	70 (21)	0.06	0.67	265	29	934	35	288	5	302	4.2	2	12	2	87
2T1B1	140 (43)	0.07	0.95	190	21	937	30	329	9	361	1.4	0.6	10	3	87
2T1B2	140 (43)	0.06	0.70	330	19	1012	38	274	7	290	2.4	0.5	19	2	78
2T1B3	140 (43)	0.06	0.97	150	46	866	28	362	8	388	1.2	0.6	4	68	28
2T2B1	140 (43)	0.06	0.67	720	10	1317	95	279	8	297	4.2	0.5	30	12	58
2T2B2	140 (43)	0.06	0.87	200	21	856	42	320	5	336	1.9	0.6	15	4	81
2T2B3	140 (43)	0.05	0.62	165	20	1264	54	286	12	311	4.6	0.7	13	1	86
2T3B1	140 (43)	0.05	0.63	145	7	942	46	258	8	289	2.3	0.3	32	38	31
2T3B2	140 (43)	0.06	0.58	160	13	1222	28	268	7	300	2.5	0.9	28	10	62
2T3B3	140 (43)	0.05	0.73	195	27	1086	52	280	9	301	1.7	0.5	23	2	76
3T1B1	200 (61)	0.07	0.73	230	12	1039	27	288	6	313	1.4	0.4	21	18	62
3T1B2	200 (61)	0.07	0.70	800	16	1231	32	280	12	316	3.4	1.3	16	1	83
3T1B3	200 (61)	0.07	0.70	115	36	1003	58	305	12	343	2.1	1	7	38	56
3T2B1	200 (61)	0.06	0.53	275	6	1589	132	266	9	291	4.7	1	30	13	57
3T2B2	200 (61)	0.07	0.81	220	20	1068	81	342	18	401	4.4	1.4	15	9	76
3T2B3	200 (61)	0.07	0.52	290	17	1348	179	301	6	314	4.5	0.3	17	1	82
3T3B1	200 (61)	0.06	0.32	540	9	1485	71	268	8	291	3.8	0.7	29	32	37
3T3B2	200 (61)	0.06	0.49	240	12	1330	98	270	7	297	3.8	1	25	7	68
3T3B3	200 (61)	0.06	0.6	165	24	1411	66	294	13	345	5.4	1.5	17	3	79
4T1B1	300 (91)	0.07	0.68	1100	12	1969	139	242	9	275	8	2.4	31	11	59
4T1B2	300 (91)	0.07	0.69	240	37	1251	91	309	9	350	2.8	0.7	6	24	70
4T1B3	300 (91)	0.08	0.77	345	48	2097	756	361	10	386	5	0.5	2	85	14
4T2B1	300 (91)	0.07	0.74	210	10	1173	35	306	14	350	4.3	1.1	11	13	76
4T2B2	300 (91)	0.07	0.60	125	13	1750	500	329	6	357	9.5	1.2	13	9	78
4T2B3	300 (91)	0.06	1.03	435	30	1202	81	340	22	380	6.8	2	4	43	52
4T3B1	300 (91)	0.07	0.46	325	10	1366	112	247	8	283	2.7	1.3	30	57	12
4T3B2	300 (91)	0.06	0.57	365	29	1327	221	275	11	311	3.2	0.6	34	21	45
4T3B3	300 (91)	0.06	0.59	235	77	1317	243	314	9	343	4.8	1.2	2	94	4

creased. The diver/welders indicated the arc stability and slag behavior were not a problem for electrodes with REM addition. It is possible the addition of REM influenced the separation of oxide inclusions from the molten pool to the slag, resulting in incomplete removal of the oxides from the weld pool. Another possibility is the slag chemistry was altered in a way that increased the transfer of oxygen and hydrogen to the weld pool. The potential influence of slag chemistry will be further elaborated.

As discussed in the introduction, porosity in underwater wet welds may be formed by molecular hydrogen (Refs. 1, 3, 4) or by carbon monoxide or water vapor (Ref. 11). Formation of carbon monoxide or water vapor by oxidation reactions in the weld pool should be minimized by addition of strong deoxidants. In the present investigation, increasing titanium and REM additions increased the porosity of wet welds rather than reducing porosity. Therefore, it is most likely

porosity in wet welds is caused mainly by evolution of molecular hydrogen from the weld pool and carbon monoxide and water vapor play a lesser role.

In light of the evidence that porosity in wet welds is caused by hydrogen, it is important to consider factors that influence the transfer of hydrogen to the weld pool. Medeiros and Liu demonstrated hydrogen content of underwater wet welds is directly related to the solubility of water vapor in the slag (Ref. 6). Based on the model proposed by Medeiros and Liu, the concentrations of both hydrogen and oxygen in the weld pool are expected to be proportional to the concentration of hydroxyl ions (solubility of water vapor) in the slag. It has also been shown slag basicity influences water vapor solubility in many slag systems (Ref. 7).

To explore the possibility that slag basicity may influence the hydrogen content of the weld pool and, therefore, the porosity of the weld metal, the basicity index of some slag samples was calculated

from chemical analysis of the deposited slag. Equation 3 was employed to calculate slag basicity. Metallic elements reported in the elemental chemical analysis were assumed to be present in the form of oxides with the stoichiometry given in Table 9. Cerium, lanthanum, and boron oxides were neglected in calculation of slag basicity because they were present in low concentrations.

Results of the analysis are given in Table 9. The formulations 1T1B2 and 3T1B2 had the same coating composition, but the welds were produced at depths of 70 and 200 ft (21 and 61 m), respectively. The effect of increased depth on the slag composition was mainly an increase in the iron-oxide content, resulting in a slightly more basic slag.

Slag basicity was greatest for the formulation with ferro-manganese addition alone, intermediate for the formulation with titanium-boron additions, and least for the formulation with REM additions. The main effect of titanium-boron addi-

Table 6 — Analysis of Steel V-Groove Welds with Ti-B Additions

ID	Depth ft (m)	C wt-%	Mn wt-%	Ti ppm	B ppm	O ppm	+/-	Hardness			Porosity		Microstructure		
								Avg (HV)	+/-	Max.	Avg (%)	+/-	PF (%)	FS (%)	AF (%)
1T2B2	70 (21)	0.05	1.03	330	22	818	19	296	13	325	0.8	0.3	12	0	88
2T3B3	140 (43)	0.05	0.51	95	14	1119	9	260	9	289	3.5	1.6	29	4	67
3T1B1	200 (61)	0.05	0.6	75	8	1180	70	286	9	308	1.8	0.4	18	8	74
4T3B2	300 (91)	0.06	0.48	145	20	1223	63	226	8	251	4.0	1.6	34	9	57

Table 7 — Analysis of Steel Test Welds with REM Additions

ID	Depth ft (m)	C wt-%	Mn wt-%	Si wt-%	Ti ppm	B ppm	O ppm	+/-	Hardness			Porosity		Microstructure		
									Avg (HV)	+/-	Max.	Avg (%)	+/-	PF (%)	FS (%)	AF (%)
1R1	70 (21)	0.05	0.45	0.45	175	11	1310	139	275	4	291	4.5	1.4	22	1	77
1R2	70 (21)	0.05	0.39	0.48	325	8	1509	117	271	7	283	5.6	1.7	18	4	79
1R3	70 (21)	0.05	0.36	0.54	355	8	1657	203	262	6	280	4.2	0.3	18	3	79
2R1	140 (43)	0.04	0.39	0.35	180	10	1937	90	255	10	289	5.0	1.5	19	25	55
2R2	140 (43)	0.04	0.16	0.19	175	6	2556	72	260	9	285	7.7	0.7	16	34	50
2R3	140 (43)	0.04	0.27	0.34	215	5	2394	319	248	10	277	8.3	2.5	43	21	36
3R1	200 (61)	0.06	0.55	0.39	330	11	1841	162	241	9	271	5.5	0.5	29	15	56
3R2	200 (61)	0.06	0.17	0.30	300	5	2211	273	235	15	286	6.7	1.6	46	25	29
3R3	200 (61)	0.05	0.26	0.30	230	5	2476	98	221	12	262	6.0	0.3	54	31	15
4R1	300 (91)	0.05	0.47	0.36	375	14	1816	102	255	7	276	4.8	1.7	28	10	62
4R2	300 (91)	Did not produce a deposit														
4R3	300 (91)	Did not produce a deposit														

Table 8 — Analysis of Steel V-Groove Welds with REM Additions

ID	Depth ft (m)	C wt-%	Mn wt-%	Si wt-%	Ti ppm	B ppm	O ppm	+/-	Hardness			Porosity		Microstructure		
									Avg (HV)	+/-	Max.	Avg (%)	+/-	PF (%)	FS (%)	AF (%)
1R1	70 (21)	0.05	0.50	0.48	240	16	1565	179	248	5	262	5.3	0.8	17	5	78
2R1	140 (43)	0.05	0.23	0.40	260	14	2533	239	237	9	265	9.1	1.1	30	13	57
3R1	200 (61)	0.05	0.62	0.36	600	12	2010	285	249	7	272	7.1	0.7	34	6	59

Table 9 — As-Deposited Slag Compositions for Selected Formulations (wt-%)

ID	Depth ft (m)	Al ₂ O ₃	SiO ₂	ZrO ₂	K ₂ O	Na ₂ O	CaO	TiO ₂	MnO	FeO	B ₂ O ₃	Ce ₂ O ₃	La ₂ O ₃	BI ^(a)
3F3	200 (61)	3.2	18.5	6.5	0.38	0.3	4.3	22.0	20.8	24.0	0.0	—	—	0.80
1T1B2	70 (21)	4.0	20.1	8.1	0.53	0.4	4.8	27.1	21.6	13.3	0.0	—	—	0.58
3T1B2	200 (61)	3.8	20.2	7.4	0.48	0.3	4.5	25.5	21.3	16.6	0.0	—	—	0.63
3R2	200 (61)	3.7	20.4	7.6	0.44	0.3	4.7	26.4	14.4	20.9	0.0	0.69	0.52	0.59

(a) Basicity Index from Equation 3.

tion was to increase titanium-oxide content and decrease the iron-oxide content of the slag, which resulted in decreased slag basicity compared to the Fe-Mn formulation. The effect of REM addition was a further decrease in basicity due to a slightly higher titanium-oxide content and slightly lower combined manganese and iron-oxide content compared to the titanium-boron formulation.

Porosity is plotted as a function of slag basicity in Fig. 9. Porosity of the weld metal decreases as the slag basicity is adjusted toward a more neutral value. The

trend is consistent with the findings of Rissone *et al.* (Ref. 10), and Surian (Ref. 9) presented in Fig. 1 and the findings of Medeiros and Liu (Ref. 6) presented in Fig. 2 where weld metal hydrogen content was reduced by increasing the basicity of an acid slag toward a more neutral value. The limited amount of data from the present investigation is not sufficient to solidly confirm the effect of slag basicity on porosity in wet welds; however, due to the presence of supporting data from the literature and the importance of porosity to the quality of wet welds, further inves-

tigation may be warranted.

Based on the mechanism proposed by Medeiros and Liu (Ref. 6) for transfer of both hydrogen and oxygen to the weld metal from water vapor dissolved in the slag, it can be anticipated both oxygen and porosity would be controlled by water vapor solubility in the slag. Porosity is plotted as a function of weld metal oxygen in Fig. 10. In general, formulations that produced low levels of weld metal oxygen also produced less porous welds and porous welds were associated with high weld metal oxygen contents.

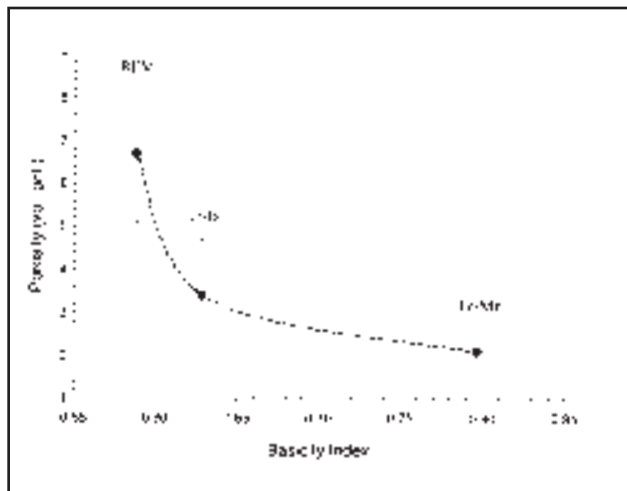


Fig. 9 — Weld metal porosity as a function of slag basicity.

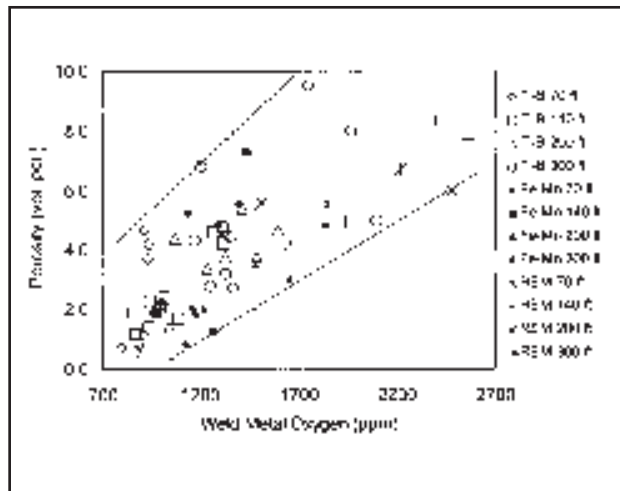


Fig. 10 — Weld metal porosity as a function of weld metal oxygen content for Task 1, 2, and 3 test welds.

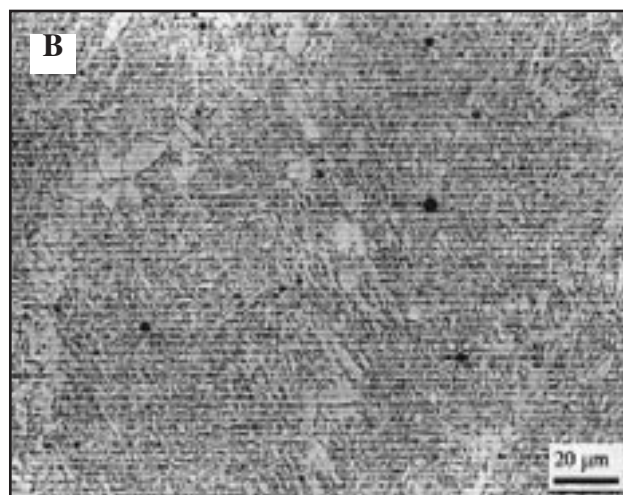
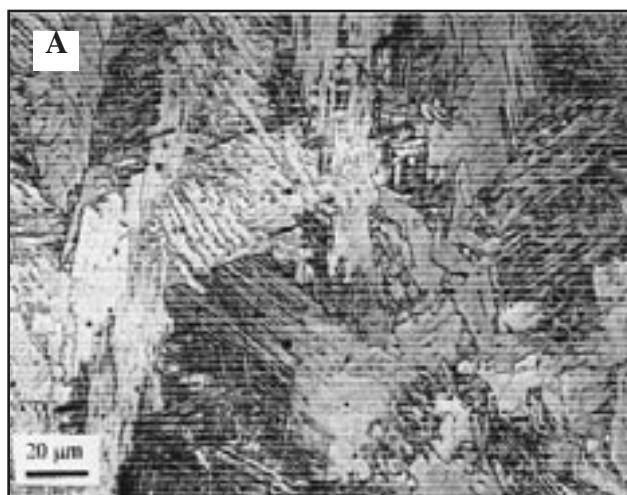


Fig. 11 — As-deposited microstructure. A — With ferro-manganese addition to the rutiled-based coating; B — with titanium-boron and ferro-manganese addition to the coating.

The trend suggests porosity and weld metal oxygen may be controlled by the same variable; thus, both may be influenced by slag basicity.

Radiography

Of the six V-groove welds produced in Task 1 with ferro-manganese additions, five met the requirements of an AWS D3.6 Class B weld in terms of porosity by radiographic inspection (Ref. 2). All of the V-groove welds produced in Task 2 with titanium-boron additions met the Class A requirements for radiographic inspection. Class A requirements are more stringent in terms of the number and size of pores allowed. Task 2 welds had less porosity overall and fewer large pores

than Task 1 welds. The higher levels of titanium-boron additions increased porosity overall, as indicated in Fig. 7, but by selecting the lowest levels of titanium and boron necessary to produce the desired microstructure, it was possible to produce V-groove welds with low porosity. Radiography of the Task 3 V-groove welds with REM additions indicated higher levels of porosity than Task 1 or Task 2 welds, which is consistent with porosity measurements by metallography.

As-Deposited Microstructure

The results of quantitative metallography are presented in Tables 3 through 8. Quantitative metallography of the as-deposited microstructure revealed a

fairly constant microstructure as a function of ferro-manganese addition for Task 1 welds that is consistent with the observation that weld metal chemical composition did not change with increasing ferro-manganese additions.

Titanium-boron additions were anticipated to produce an increase in the acicular ferrite content of the top bead microstructure. Boron retards the nucleation of ferrite on the austenite grain boundaries, allowing sufficient undercooling for intragranular nucleation of ferrite to occur. Titanium protects boron from oxidation and produces a fine distribution of titanium-rich oxide inclusions, which provide sites for the nucleation of acicular ferrite. The microstructure of the welds with only ferro-

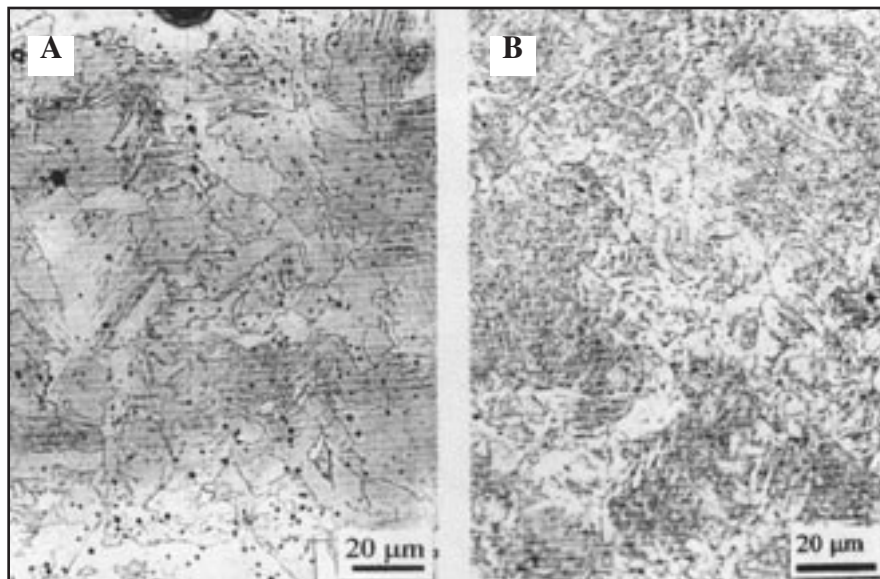


Fig. 12 — Microstructure of the coarse-grained reheated zone. A — With ferro-manganese addition to the rutile-based coating; B — with titanium-boron and ferro-manganese addition to the coating.

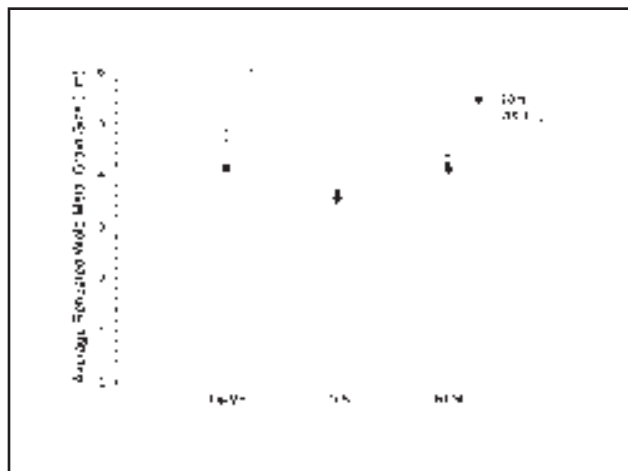


Fig. 13 — Ferrite grain size in the reheated weld metal of selected V-groove welds as a function of ferro-alloy addition and depth.

manganese addition consisted of 25–40% PF, 40–60% FS, and 10–20% AF. With titanium-boron addition, microstructures containing 60–80% AF were produced over the range of depths tested. The as-deposited top bead microstructures are shown in Fig. 11.

With REM additions, a microstructure high in AF was produced to a depth of 300 ft (91 m) despite the higher oxygen contents and lower alloy recoveries than anticipated. The AF content of the top bead microstructure is significantly greater than those of the V-groove welds with ferro-manganese additions alone.

of reheated weld metal in the multipass welds. It is anticipated the mechanical properties of underwater wet welds will be strongly influenced by the microstructure of the reheated weld metal. The three ferro-alloy additions significantly influenced the microstructure of the reheated weld metal.

The microstructure of the coarse-grained reheated zone (CGRHZ) was refined by titanium-boron additions. The CGRHZ is heated high into the austenite phase field, and significant austenite grain growth results. On cooling, the austenite transforms back to ferrite. In

The ability of the REM consumables to produce a microstructure high in AF indicates the microstructure of wet welding consumables with titanium-boron additions are fairly tolerant of variations in chemical composition and the degree of oxidation of the weld metal.

Reheated Microstructure

Underwater wet welds are typically made with small-diameter electrodes using a stringer-bead technique. As a result, there is a large frac-

tion of the welds with only ferro-manganese addition, hardenability was low and the result was a microstructure of coarse PF with a small amount of FS, as seen in Fig. 12A. In welds with titanium-boron addition, the microstructure in the CGRHZ consisted of a much smaller amount of PF on the prior-austenite grain boundaries, and intragranular AF and FS, as seen in Fig. 12B. Titanium addition also increased the recovery of manganese. Higher manganese contents increase hardenability and promote intragranular nucleation of ferrite. The result was a much finer ferrite microstructure in the CGRHZ for welds with titanium-boron additions compared to welds with ferro-manganese additions alone.

Microstructural refinement was also apparent in the fine-grained reheated zone (FGRHZ), although not to the same extent as in the CGRHZ. The FGRHZ is heated to low temperatures in the austenite phase field where there is little opportunity for austenite grain growth. The grain size in the FGRHZ is more closely related to the as-deposited microstructure from which it originated. Refinement of the FGRHZ microstructure occurred due to the finer as-deposited microstructure in the titanium-boron welds.

The average ferrite grain size of the reheated weld metal for six selected V-groove welds is presented in Fig. 13. The finest ferrite grain size occurred in the titanium-boron-containing welds, while the ferro-manganese- and REM-containing welds had a coarser ferrite grain size in the reheated weld metal. The reheated weld metal grain size is refined with higher hardenability and the yield strength increases with finer grain size. Greater depths produced a slightly coarser grain size due to reduced hardenability with increased oxidation of the weld pool.

Mechanical Properties

The mechanical properties of V-groove welds are presented in Tables 10–12. Tensile strengths were higher in all cases for welds with titanium-boron additions than for welds with only ferro-manganese additions. Ultimate tensile strengths were brought up above 60 ksi at 200 and 300 ft (61 and 91 m) with titanium-boron additions, which is an improvement over the lower values produced with only ferro-manganese additions. The increase in strength was due to a combination of microstructural refinement and solid solution strengthening. Tensile strengths of Task 3 welds with REM additions were lower than those of welds with only titanium-boron additions. The decrease in strength was due to

an increase in reheated weld metal grain size and a reduction in solid solution strengthening compared to the welds with only titanium-boron additions.

Although significant microstructural refinement occurred as a result of titanium-boron addition, little or no improvement in Charpy impact toughness at 28°F (-2°C) was observed. Microstructural refinement is known to shift the ductile to brittle transition to lower temperatures, giving a greater margin of safety from brittle fracture. In the present investigation, impact toughness measurements were made at only one temperature and analysis in the electron microscope revealed all of the Charpy bars fractured by ductile void coalescence over 90 to 100% of the fracture surface. All impact toughness values reported are on the upper shelf; therefore, if any reduction in the Charpy transition temperature occurred it was not observed.

Upper shelf toughness is controlled by the concentration of defects and is not as sensitive to changes in microstructure as is transition temperature. In surface welds, upper shelf toughness is strongly influenced by weld metal oxygen content. Oxide inclusions act as sites for initiation of ductile void coalescence. It is likely the upper shelf toughness of underwater wet welds is limited by the high concentration of defects such as pores, oxide inclusions, and microcracks, and is not highly sensitive to microstructure. The low-impact toughness values of the welds made with REM addition can be attributed to high volume fraction of porosity.

Tensile elongation values are low compared to steel surface welds of similar strength levels, but are not atypical for underwater wet welds made at these depths. The presence of porosity, oxide inclusions, and microscopic cracks causes a reduction in ductility of underwater wet welds compared to surface welds. Hydrogen is certainly present in weld metal deposited under water and may also play a role in reducing ductility. The present investigation was a development effort; it is noted additional mechanical testing and a full procedure qualification, including bend tests, would need to be performed in order to determine fitness for service for specific engineering applications. Nevertheless, it is known in the welding community that actual repairs have been made on marine structural failures with consumables that exhibit properties similar to those generated herein.

Conclusions

1) The chemical composition of steel underwater wet welds can be controlled by addition of a strong deoxidant, such as

Table 10 — Results of Mechanical Testing on Steel Underwater Wet Welds with Increasing Ferro-Manganese Additions to the Coating of a Rutile-Based Electrode

ID	Depth ft (m)	All-Weld-Metal Tensile			Charpy Impact Toughness @28°F (-2°C) ft-lb (J)			
		Yield Stress ksi (MPa)	Ultimate Stress ksi (MPa)	Elongation (%)	Average	Min.	Max.	Percent Shear Fracture
1F3	70 (21)	64 (441)	71 (489)	18.6	29 (39)	28 (38)	30 (41)	90
2F3	140 (43)	56 (386)	65 (448)	11.7	25 (34)	23 (31)	28 (38)	100
3F3	200 (61)	53 (365)	59 (407)	3.6	23 (31)	22 (30)	24 (33)	100
4F2	300 (91)	54 (372)	59 (407)	6.8	19 (26)	17 (23)	20 (27)	100

Table 11 — Results of Mechanical Testing on Steel Underwater Wet Welds with Titanium-Boron and Ferro-Manganese Additions to the Coating of a Rutile-Based Electrode

ID	Depth ft (m)	All-Weld-Metal Tensile			Charpy Impact Toughness @28°F (-2°C) ft-lb (J)			
		Yield Stress ksi (MPa)	Ultimate Stress ksi (MPa)	Elongation (%)	Average	Min.	Max.	Percent Shear Fracture
1T2B2	70 (21)	67 (462)	71 (489)	4.2	22 (30)	21 (29)	24 (33)	90-100
2T3B3	140 (43)	78 (537)	80 (551)	3.7	26 (35)	24 (33)	30 (41)	100
3T1B1	200 (61)	64 (441)	68 (469)	6.4	22 (30)	22 (30)	22 (30)	100
4T3B2	300 (91)	57 (393)	60 (413)	8.7	20 (27)	19 (26)	20 (27)	100

Table 12 — Results of Mechanical Testing on Steel Underwater Wet Welds with Rare Earth Metal, Titanium-Boron, and Ferro-Manganese Additions to Coating of a Rutile-Based Electrode

ID	Depth ft (m)	All-Weld-Metal Tensile			Charpy Impact Toughness @28°F (-2°C) ft-lb (J)			
		Yield Stress ksi (MPa)	Ultimate Stress ksi (MPa)	Elongation (%)	Average	Min.	Max.	Percent Shear Fracture
1R1	70 (21)	70 (482)	75 (517)	6.8	24 (33)	20 (27)	27 (37)	90-100
2R1	140 (43)	57 (393)	61 (420)	5.0	14 (19)	12 (16)	16 (22)	80-100
3R1	200 (61)	57 (393)	63 (434)	5.0	18 (24)	16 (22)	19 (26)	100
4R1	300 (91)	55 (379)	59 (406)	4.3	17 (23)	16 (22)	20 (27)	80-100

titanium, to the system, which will protect weaker oxide formers, such as manganese, from oxidation.

2) Acid-type slags produced greater levels of porosity, which is assumed to be caused by hydrogen, and weld metal oxygen than more neutral-type slags. This effect may be related to the minimum in water-vapor solubility in slags near neutral basicity.

3) Additions of titanium and boron are effective at refining the ferrite grain size of the as-deposited and reheated microstructures of steel wet welds over the range of depths tested, 70 to 300 ft (21 to 91 m). The proportion of acicular ferrite (AF) in the as-deposited microstructure

was significantly increased through titanium-boron additions (60-80% AF) over welds with only ferro-manganese additions (10-20% AF).

4) Combined additions of titanium, boron, and manganese increased the tensile strength of the steel wet welds due to microstructural refinement.

5) The degree of microstructural refinement and reduction in weld metal oxygen content produced by titanium-boron additions did not significantly improve Charpy impact toughness at 28°F (-2°C). Upper-shelf toughness of wet welds is most likely controlled by the concentration of defects, such as pores, microcracks, and oxide inclusions.

Acknowledgments

The authors would like to thank Amoco, Chevron, Exxon, Mobil, and the Minerals Management Service for funding this research.

References

1. Suga, Y., and Hasui, A. 1986. On formation of porosity in underwater wet weld metal (the first report). *Transactions of the Japan Welding Society* 17(1): 58-64.
2. ANSI/AWS D3.6M, *Specification for Underwater Welding*. 1999. Miami, Fla.: American Welding Society,
3. Ando, S., and Asahani, T. 1983. A study on the metallurgical properties of steel welds with underwater gravity welding. *Proc. Conf.: Underwater Welding*. International Institute of Welding, Pergamon Press.
4. Suga, Y. 1987. Blowhole formation by hydrogen. *Transactions of the Japan Welding Society* 18(1): 61-68.
5. Sanchez-Osio, A., Liu, S., and Ibarra, S. 1995. Designing shielded metal arc consumables for underwater wet welding in offshore applications. *Journal of Offshore Mechanics and Arctic Engineering* 117(3): 212-220.
6. Medeiros, R., and Liu, S. 1998. A predictive electrochemical model for weld metal hydrogen pickup in underwater wet welds. *Journal of Offshore Mechanics and Arctic Engineering* 120(4): 243-248.
7. Turkdogan, E. T. 1983. *Physiochemical Properties of Molten Slags and Glasses*. London, U.K.: The Metals Society.
8. Tuliani, S. S., Boniszewski, T. and, Eaton, N. F. 1969. Notch toughness of commercial submerged arc weld metal. *Welding and Metal Fabrication* (8): 327-339.
9. Surian, E. 1997. ANSI/AWS E7024 SMAW electrodes: the effect of coating magnesium additions. *Welding Journal* 76(10): 404-s to 411-s.
10. Rissone, N., Bott, I., Jorge, J., Corvalan, P., and Surian, E. 1997. ANSI/AWS A5.1-91 E6013 rutile electrodes: the effect of Wollastonite. *Welding Journal* 76(11): 498-s to 507-s.
11. Liu, S., Olson, D. L., and Ibarra, S. 1994. Electrode formulation to reduce weld metal hydrogen and porosity. *Proc. 13th Offshore Mechanics and Arctic Engineering Conf.* American Society of Mechanical Engineers.
12. *Guide to Light Microscope Examination of Ferritic Steel Weld Metals*. IIW Doc. No. IX-1533-88. International Institute of Welding, American Council, AWS, Miami, Fla.

Preparation of Manuscripts for Submission to the *Welding Journal* Research Supplement

All authors should address themselves to the following questions when writing papers for submission to the *Welding Research Supplement*:

- ◆ Why was the work done?
- ◆ What was done?
- ◆ What was found?
- ◆ What is the significance of your results?
- ◆ What are your most important conclusions?

With those questions in mind, most authors can logically organize their material along the following lines, using suitable headings and subheadings to divide the paper.

1) **Abstract.** A concise summary of the major elements of the presentation, not exceeding 200 words, to help the reader decide if the information is for him or her.

2) **Introduction.** A short statement giving relevant background, purpose and scope to help orient the reader. Do not duplicate the abstract.

3) **Experimental Procedure, Materials, Equipment.**

4) **Results, Discussion.** The facts or data obtained and their evaluation.

5) **Conclusion.** An evaluation and interpretation of your results. Most often, this is what the readers remember.

6) **Acknowledgment, References, and**

Appendix.

Keep in mind that proper use of terms, abbreviations and symbols are important considerations in processing a manuscript for publication. For welding terminology, the *Welding Journal* adheres to ANSI/AWS A3.0:2001, *Standard Welding Terms and Definitions*.

Papers submitted for consideration in the *Welding Research Supplement* are required to undergo Peer Review before acceptance for publication. Submit an original and one copy (double-spaced, with 1-in. margins on 8 1/2 x 11-in. or A4 paper) of the manuscript. Submit the abstract only on a computer disk. The preferred format is from any Macintosh® word processor on a 3.5-in. double- or high-density disk. Other acceptable formats include ASCII text, Windows™ or DOS. A manuscript submission form should accompany the manuscript.

Tables and figures should be separate from the manuscript copy and only high-quality figures will be published. Figures should be original line art or glossy photos. Special instructions are required if figures are submitted by electronic means. To receive complete instructions and the manuscript submission form, please contact the Peer Review Coordinator, Doreen Kubish, at (305) 443-9353 ext. 275; FAX (305) 443-7404; or write to the American Welding Society, 550 NW LeJeune Rd., Miami, FL 33126.